Development 139, 2681-2691 (2012) doi:10.1242/dev.078345

Genome-wide analysis reveals that Smad3 and JMJD3 HDM co-activate the neural developmental program

Conchi Estarás[1], Naiara Akizu[1,*], Alejandra García[1], Sergi Beltrán[2,‡], Xavier de la Cruz[3,§,¶] and Marian A. Martínez-Balbás[1,¶]

SUMMARY

Neural development requires crosstalk between signaling pathways and chromatin. In this study, we demonstrate that neurogenesis is promoted by an interplay between the TGFβ pathway and the H3K27me3 histone demethylase (HDM) JMJD3. Genome-wide analysis showed that JMJD3 is targeted to gene promoters by Smad3 in neural stem cells (NSCs) and is essential to activate TGFβ-responsive genes. In vivo experiments in chick spinal cord revealed that the generation of neurons promoted by Smad3 is dependent on JMJD3 HDM activity. Overall, these findings indicate that JMJD3 function is required for the TGFβ developmental program to proceed.

KEY WORDS: Histone demethylation, Epigenetic regulation, JMJD3 (Kdm6b), Smad3, TGFβ pathway, Neurogenesis

INTRODUCTION

Epigenetic mechanisms that regulate access to the genetic material govern cell differentiation and embryonic development. This epigenetic control is mainly mediated by covalent modifications of histones and DNA (Kouzarides, 2007). Recently, histone methylation has received special attention as an essential regulator of gene expression. In particular, methylation of lysine 27 of histone H3 (H3K27me3) has been found to be an important regulator of embryonic development and cell homeostasis (Margueron and Reinberg, 2010; Morey and Helin, 2010). The enzymes responsible for this activity are enhancer of zeste homologs 1 and 2 (EZH1/2) (Cao et al., 2002; Czermin et al., 2002; Kuzmichev et al., 2002). H3K27me3 is recognized by the chromodomain of the polycomb protein that forms part of PRC1 (Cao et al., 2002; Lois et al., 2010). The recruitment of PRC1 leads to final transcriptional repression (Cao et al., 2002), a state that can be reversed by the removal of H3K27me3 marks by Jumonji C (JmjC) domain-containing proteins, JMJD3 and UTX histone demethylases (Agger et al., 2007; De Santa et al., 2007; Lan et al., 2007; Lee et al., 2007). The importance of the balance between methyltransferase and demethylase activity is reflected by the fact that many key developmental promoters are often marked by H3K27me3 (Boyer et al., 2006; Bracken et al., 2006; Lee et al., 2006; Pan et al., 2007). Indeed both UTX and JMJD3 derepress HOX genes and a subset of neural and epidermal differentiation genes (Agger et al., 2007; Burgold et al., 2008; Jepsen et al., 2007; Lan et al., 2007; Lee et al., 2007; Sen et al., 2008). In particular, UTX is enriched around the transcription start sites of many HOX genes in primary human fibroblasts, which correlates with a strong decrease in H3K27me3 levels. However, in embryonic stem cells (ESCs), in which these genes are repressed, UTX is excluded from the HOX loci (Agger et al., 2007; Lan et al., 2007). In addition, inhibition of a zebrafish UTX homolog or the *Caenorhabditis elegans* JMJD3 ortholog leads to mis-regulation of HOX genes and developmental defects (Agger et al., 2007; Lan et al., 2007). However, in isolated cortical progenitor cells, SMRT prevents retinoic-neuronal differentiation by repressing the expression of JMJD3, which can activate specific components of the neurogenic program (Jepsen et al., 2007). These findings show an important contribution of JMJD3/UTX during development. However, in spite of the essential role of H3K27me3 and its demethylases during development, we do not know how they respond to developmental signals.

Signaling pathways are essential during development. Specifically, transforming growth factor β (TGFβ) signaling is important for both embryonic development and tissue homeostasis (Moustakas and Heldin, 2009). At the cellular level, TGFβ regulates cell growth, differentiation, adhesion, migration and death in a cell context-dependent manner (Yang and Moses, 2008). However, alterations in TGFβ signaling lead to congenital malformations, inflammation and cancer (reviewed by Gordon and Blobe, 2008; Massague et al., 2005). Mechanistically, TGFβ transduces signals from the plasma membrane by interacting with type I and type II receptors, which are serine/threonine kinases. Cytokine binding induces phosphorylation and activation of Smad2 and Smad3 at C-terminal serine residues, while activated Smad2/3 proteins interact with Smad4 to enter the nucleus and regulate gene expression (Feng and Derynck, 2005; Shi and Massague, 2003; Varga and Wrana, 2005). The biological output of TGFβ pathway activation depends on the subset of genes that are regulated in each cellular context (Massague, 2000), which, in turn, varies with each particular combination of co-factors. Specific chromatin modifier enzymes have been associated with activated Smad proteins, such as histone acetyltransferases P/CAF, CBP/p300 or the ATP-dependent remodeling factor Brg1 (Feng and Derynck, 2005; Massague et al., 2005; Xi et al., 2008). In particular, the TGFβ

[1]Department of Molecular Genomics, Instituto de Biología Molecular de Barcelona (IBMB), Consejo Superior de Investigaciones Científicas (CSIC), 08028 Barcelona, Spain. [2]Unitat de Bioinformàtica, Centres Científics i Tecnològics–Universitat de Barcelona, 08028 Barcelona, Spain. [3]Department of Structural Biology, Instituto de Biología Molecular de Barcelona (IBMB-CSIC), Institut Català per la Recerca i Estudis Avançats (ICREA), Parc Científic de Barcelona, 08028 Barcelona, Spain.

*Present address: Department of Neurosciences and Pediatrics. University of California, San Diego. La Jolla, CA 92093-0665, USA.
‡Present address: Centre Nacional d'Anàlisi Genòmica (CNAG), Parc Científic de Barcelona; 08028 Barcelona, Spain.
§Present address: Vall d'Hebron Institute of Research (VHIR), Passeig de la Vall d'Hebron, 119; E-08035 Barcelona, Spain.
¶Authors for correspondence (xdmcri@ibmb.csic.es; mmbbmc@ibmb.csic.es)

Accepted 8 May 2012

effectors Smad2/3 interact with JMJD3 to de-repress certain loci in ESCs (Dahle et al., 2010; Kim et al., 2011). Here, we demonstrate by genome-wide analysis and in vivo experiments that TGFβ-neural development-associated function requires JMJD3 activity.

The results of the present study show by ChIP-Seq analysis that JMJD3 and Smad3 colocalize at the transcriptional start site (TSS) of TGFβ responsive genes in neural stem cells (NSCs). Moreover, genome-wide expression profiling reveals that the neural developmental targets of TGFβ signaling require JMJD3 for proper regulation. Finally, in vivo experiments in chick developing spinal cord demonstrate that JMJD3 activity is essential for Smad3-induced neuronal differentiation.

MATERIALS AND METHODS

Cell culture and CoIP assays

Human 293t cells were grown under standard conditions (Blanco-Garcia et al., 2009). Mouse NSCs, provided by Dr K. Helin (University of Copenhagen, Denmark), were dissected out from cerebral cortex of mouse embryos (E12.5) and cultured in a poly-D-lysine (5 μg/ml, 2 hours at 37°C) and laminin (5 μg/ml, 4 hours at 37°C) pre-coated dishes growing with a media comprising equal parts DMEM F12 (without Phenol Red, Gibco) and Neural Basal Media (Gibco) containing penicillin/streptomycin and Glutamax (1%), N2 and B27 supplements (Gibco), non essential amino acids (0.1 mM), sodium pyruvate (1 mM), Hepes (5 mM), heparin (2 mg/l), bovine serum albumin (25 mg/l) and β-mercaptoethanol (0.01 mM). We added fresh recombinant human EGF (R&D Systems) and FGF (Invitrogen) to 20 ng/ml and 10 ng/ml final, respectively. NSCs preserve the ability to self-renew and to generate a wide range of differentiated neural cell types (Calloni et al., 2009; Gossrau et al., 2007; Sasaki et al., 2006). TGFβ (Millipore) was used at a final concentration of 5 ng/ml. CoIP experiments were carried out as described previously (Akizu et al., 2010).

Plasmids and recombinant proteins

Flag-Smad2, Flag-Smad3 and Flag-Smad3S/D cloned into pCIG vector were kindly provided by Dr E. Martí (Garcia-Campmany and Marti, 2007). pCIG-Myc-JMJD3 and pCIG-Myc-JMJD3 DN have been previously described (Akizu et al., 2010). shRNA against chicken JMJD3 was cloned in pShin vector (Kojima et al., 2004). shRNA against mouse JMJD3 was cloned into pLKO.1-puro vector and it was purchased from Sigma [shJMJD3(2837), TRCN0000095265]. GST-Smad3 full-length and GST-Smad3 MH1 domain (1-155) were kindly provided by Dr J. Massagué (Xu et al., 2003). GST-Smad3 MH2 (199-425) and Linker-MH2 (146-425) domains were acquired from Addgene.

Antibodies and reagents

TGFβ was acquired from Millipore (GF111). Antibodies used were: mouse anti-Smad3 (Abcam 55480), rabbit anti-ChIP Grade Smad3 (Abcam, 28379), rabbit anti-PhosphoSmad3 (Cell Signaling, mAb9520), mouse anti-Flag (Sigma M2), mouse anti-Nestin (BD Biosciences, 611653), mouse anti-β-Tubulin III (Tuj1, Covance, MMS-435P), rabbit anti-trimethyl H3K27 (Millipore, 07449), rabbit anti-Sox2 (Invitrogen, 48-1400), mouse anti-HuC/D (MP, A21271), rabbit anti-Gfap (Dako, z0334), rabbit anti-Id1 (Santa Cruz, sc488), rabbit anti-ph3 (Upstate, 06-570) and mouse anti-Mnr2 (DSHB, 81.5C10). Rabbit anti-JMJD3 was kindly provided by Dr K. Helin (Agger et al., 2009). Mouse anti-Myc antibody was a gift from Dr S. Pons (Instituto de Investigaciones Biomedicas de Barcelona, Spain). Guinea pig anti-Lbx1 was kindly provided by Dr E. Martí (Instituto de Biología Molecular de Barcelona, Spain).

Microarray analysis

RNAs from 10^6 non-stimulated or TGFβ-stimulated (for 2.5 hours) KD C and KD JMJD3 cells were supplied to the Microarrays Unit of the Centre for Genomic Regulation (CRG) LOCATION? for quality control, quantification, reverse transcription, labeling and hybridization using an Agilent Platform with Whole Mouse Genome microarrays. Triplicates were analyzed for untreated and TGFβ-treated KD C and KD JMJD3 samples. Fold changes (FCs) between untreated and the corresponding TGFβ-treated samples were calculated by applying the AFM tool. The list of JMJD3-dependent TGFβ-responsive genes was generated using a two-step protocol. First, we identified the genes putatively sensitive to TGFβ regulation. These were defined as those genes from the KD C with significant values (adjusted P-value ≤0.05) for the fold change between gene expression levels in TGFβ-treated and untreated cells (this fold change is abbreviated as FC). Second, we used the resulting 2744 gene set to generate the list of candidate genes. This was carried out by generating two subsets of genes: the subset of genes for which FC remains significant in the KD JMJD3 array (adjusted P-value ≤0.05) but showed a lower FC (differences larger than 25% of the corresponding FC in the KD C array); and the subset of genes with non-significant FC (P≥0.1) in the KD JMJD3 array experiment. We subsequently put these two subsets together to produce a final list of 781 candidates. Microarray data have been deposited in GEO database under Accession Number GSE35361.

ChIP assays

ChIPs from NSCs were carried out using previously described procedures (Frank et al., 2001) with modifications: 3×10^6 NSCs untreated or treated with TGFβ (5 ng/ml, for the indicated times) were fixed with di (N-succinimidyl) glutarate (DSG) 0.2 mM for 45 minutes at room temperature followed by formaldehyde (1% for 20 minutes). Fixation was stopped by addition of 0.125 mM glycine. The sonication step was performed in a Bioruptor sonicator (12 minutes and 30 seconds on, 30 seconds off). ChIP DNA was analyzed by qPCR in a LightCycler 480 PCR system (Roche). ChIPs from electroporated chick cells were essentially performed as described previously (Akizu et al., 2010).

ChIP-Seq procedure

A standard ChIP protocol was used. Before sequencing, ChIP DNA was prepared by simultaneously blunting, repairing and phosphorylating ends according to manufacturer's instruction (Illumina). The DNA was adenylated at the 3′ end and recovered by Qiaquick PCR purification kit (Qiagen) according to the manufacturer's recommendations. Adaptors were added by ligation and the ligated fragments were amplified by PCR, resolved in a gel and purified by Qiagen columns. Samples were loaded into individual lanes of flow cell. We generated almost 20 million 36 bp reads for each ChIP sample. Reads were mapped with bowtie (Langmead et al., 2009) to the UCSC (Fujita et al., 2011) *Mus musculus* genome release 9; only sequence reads mapping at unique locations were kept. Peaks were called with MACS (Zhang et al., 2008) on each sample with Input as control. Only one read from each set of duplicates was kept, P-value cutoff for peak detection was set to 1e–4 and PeakSplitter was invoked. The total number of peaks called for Smad3 and for JMJD3 were 98086 and 63154, respectively. PeakAnalyzer (Salmon-Divon et al., 2010) was used to find the closest upstream or downstream refGene Transcription Start Site (TSS). R language and Bioconductor (Gentleman et al., 2004), including packages ShortRead and IRanges (Morgan et al., 2009), were used for further annotation and statistical analysis. ChIP-Seq data have been deposited in GEO database under Accession Number GSE36673.

Size exclusion chromatography

Size exclusion chromatography was performed with whole cell extracts in a Superose-6 10/300 gel filtration column (GE Healthcare) on AKTA purifier system (GE Healthcare).

Purification of recombinant proteins and GST pull down assays

GST pull-downs were performed essentially as described previously (Valls et al., 2003).

Immunoblotting

Immunoblotting was performed using standard procedures and visualized by means of an ECL kit (Amersham).

mRNA extraction and qPCR

mRNA from NSCs was extracted with QIAGEN columns following manufacturer's instructions. mRNA from dissected neural tubes was extracted by TRIZOL (Invitrogen) protocol. qPCR was performed with Sybergreen (Roche) in LC480 Lightcycler (Roche) using the primers in supplementary material Table S2.

Indirect immunofluorescence

The brachial regions from collected embryos were fixed for 2 hours at 4°C in 4% paraformaldehyde. Indirect immunofluorescence was essentially performed as described previously (Akizu et al., 2010).

In situ hybridization

RNA in situ hybridization of whole-mount embryos was carried out following standard procedures (Schaeren-Wiemers and Gerfin-Moser, 1993) using ESTbank probes for chick JMJD3, NeuroD1, Ngn2 and Smad3.

GFP+ cell position measurement

Images from electroporated (EP) neural tubes were obtained on Leica SP5 confocal. Maximum projection of 10 sections was generated and used for quantification. Image J software was used to quantify the position of GFP^+ cells along the mediolateral axis. The Y coordinate was used to define the GFP^+ cell position respect to the lumen (Y=0). First, neural tube mediolateral axis was divided into four equal quadrants encompassing the entire Y axis (from lumen to mantle zone). Second, the Y value of each GFP^+ cell was defined. Third, GFP^+ cells were grouped in one of the quadrants according to their Y values. Finally, the percentage of GFP^+ cells in each quadrant was calculated and the average from all quantified sections was represented in the graph (Fig. 5D).

Lentiviral transduction

Lentiviral production was performed as described previously (Rubinson et al., 2003). Viral particles were added to NSCs and infected cells were selected with puromycine (1 μg/ml) 24 hours later.

Chick in ovo electroporation

In ovo electroporation experiments were performed as previously described (Akizu et al., 2010). Total EP DNA was adjusted to 3.5 μg/μl.

Statistical analysis

Quantitative data were expressed as mean and standard deviation (s.d.) of at least three biologically independent experiments. The significance of differences between groups was assessed using the Student's *t*-test (*P<0.05; **P<0.01).

RESULTS

Phosphorylated Smad3 interacts with JMJD3 in NSCs

The TGFβ signaling pathway has recently been reported to have a role in neural development (Garcia-Campmany and Marti, 2007). Besides, we know that JMJD3 regulates many developmental and, in particular, key neural promoters (Jepsen et al., 2007). Given this, we wondered whether JMJD3 cooperated in TGFβ-dependent neural development. In order to address this issue, we used a suitable neural cell model: NSCs. First, we demonstrated that JMJD3 and the phosphorylated form of Smad3 (Smad3P) co-purified in TGFβ-treated NSC extracts in a gel filtration assay (Fig. 1A). We then confirmed that JMJD3 interacts with the Smad3P by co-immunoprecipitation (Co-IP) experiments (Fig. 1B). Next, by pull-down assay, we identified that the Smad3 regions responsible for the interaction with JMJD3 are the MH1 and linker domains (Fig. 1C, lanes 3 and 5). As these are the least well-conserved domains between Smad2 and Smad3 proteins (supplementary material Fig. S1A), we tested the specificity of the JMJD3 interaction with Smad proteins. Co-IP assays showed that Smad2 did not interact with JMJD3 (supplementary material Fig. S1B,C).

We then wanted to assess whether the Smad3-JMJD3 interaction was biologically relevant for TGFβ function in NSCs. To this end, we established a JMJD3 knockdown (KD) cell line of NSCs that expresses low levels of JMJD3 without affecting Smad3 expression (Fig. 1D) and maintaining neural stem cell identity (supplementary material Fig. S2). Then, we analyzed the effects of JMJD3 depletion on the TGFβ response. As shown in Fig. 1E, TGFβ treatment of control cells led to a clear decrease in Nestin, a neural progenitor marker. By contrast, TGFβ failed to downregulate Nestin in JMJD3 KD cells. These findings suggest that changes in neural stem cell identity mediated by TGFβ depend on JMJD3.

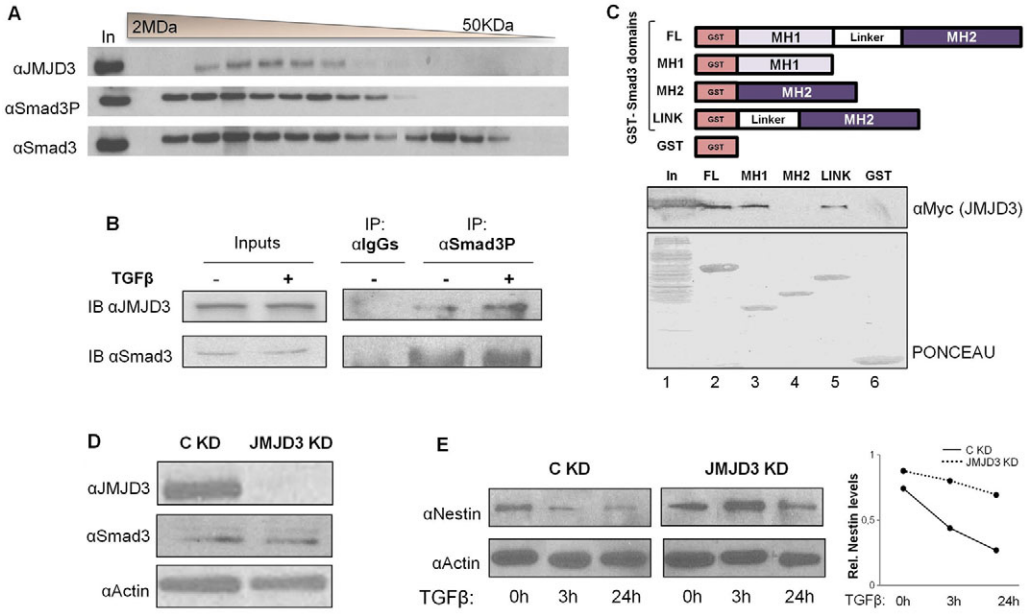

Fig. 1. Endogenous Smad3 and JMJD3 interact in NSCs. (**A**) Size-exclusion chromatography of NSC lysate showing co-elution of Smad3P and JMJD3, and the presence of Smad3 in the lower weight fractions. (**B**) Co-IP of mouse NSCs lysate using anti-Smad3P antibody or unrelated IgGs in the presence or absence of TGFβ for 30 minutes. (**C**) Upper panel shows schematic representation of GST-Smad3 fragments: full length (FL), MH1 (1-155 aa), MH2 (199-425 aa) and linker domains that also contains MH2 (146-425 aa). Pull-down assay using GST-Smad3 fusion proteins and 293t cell extracts overexpressing Myc-JMJD3. Ponceau staining of GST-Smad3 proteins (lower panel). (**D**) Immunoblot from control knockdown (C KD) and JMJD3 knockdown (JMJD3 KD) cell extracts using the indicated antibodies. (**E**) Immunoblot showing Nestin expression prior to and after TGFβ treatment for the indicated times in C KD and JMJD3 KD cells. Nestin levels (relative to Actin) were quantified by using the Image J software (graph on the right). Input (In) corresponds to 1% of the protein present in the whole-cell extract.

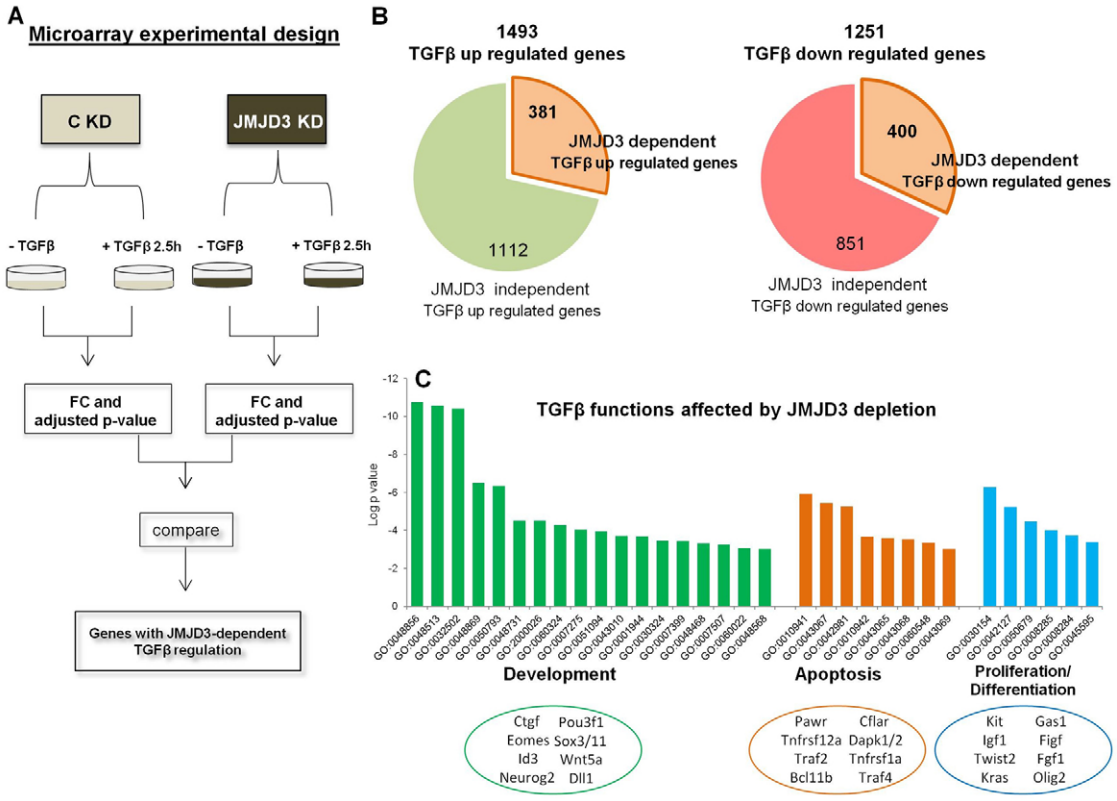

Fig. 2. TGFβ and JMJD3 regulate common target genes. (**A**) Schematic representation of microarray analysis design. (**B**) Diagrams depict the number of TGFβ-responsive genes that need JMJD3 to be efficiently upregulated (on the left) or downregulated (on the right). (**C**) GO analysis of the TGFβ-responsive genes dependent on JMJD3.

TGFβ-induced gene expression profile depends on JMJD3

To explore whether JMJD3 contributes to the TGFβ response, we set out to identify genes co-regulated by TGFβ and JMJD3. For this, we performed a microarray expression experiment with control (C KD) and JMJD3-depleted NSCs (JMJD3 KD) left untreated or treated with TGFβ for 2.5 hours (Fig. 2A). We confirmed the results of the two microarrays by qPCR of 12 genes selected to cover the whole range of changes in gene expression (supplementary material Fig. S3A). Interestingly, from 2744 TGFβ-responsive genes in control cells ($P \leq 0.05$: 1493 genes upregulated and 1251 genes downregulated, see Fig. 2B), 781 targets were not affected to the same extent by TGFβ in JMJD3-depleted cells (Fig. 2B and supplementary material Table S1). These correspond to genes regulated by TGFβ in control cells but not efficiently regulated in JMJD3-depleted cells after TGFβ treatment. Of these 781 candidates, 381 showed JMJD3 dependency for transcription activation (Fig. 2B, left panel). This was more evident for genes with larger transcriptional changes upon TGFβ treatment (75% of genes with FC≥2 were not activated in KD JMJD3 cells; supplementary material Fig. S3B), in agreement with an activating role for JMJD3. Nevertheless, JMJD3 seems to be required to direct or indirectly repress 400 TGFβ downregulated target genes (Fig. 2B, right panel). To further characterize the differences between C KD and JMJD3 KD cells in response to TGFβ signaling, we performed an enrichment analysis of Gene Ontology (GO) terms over the 781 JMJD3-dependent genes (supplementary material Table S1) to identify those biological processes most sensitive to JMJD3 levels in response to TGFβ signaling. The results of this analysis showed that the most significantly enriched GO terms were associated with development ('anatomical structure development', 'organ development' and 'developmental process' with adjusted *P*-values of 1.76e–11, 2.75e–11 and 3.86e–11, respectively) (Fig. 2C). In addition, other well-known TGFβ functions such as apoptosis or cell proliferation and differentiation were also dependent of JMJD3 (Fig. 2C). Overall, this result points to a key role for JMJD3 in the regulation of TGFβ-responsive genes, in particular genes associated with developmental processes. Interestingly, some class II basic helix-loop-helix (bHLH) proneural genes such as neurogenin 2 (*Ngn2*) and inhibitor of DNA binding 3 (*Id3*) (Fig. 2C; supplementary material Table S1), the activity of which is essential during neurogenesis, were not fully induced by TGFβ in KD JMJD3 cells.

Smad3 and JMJD3 colocalize on gene promoters

The ability of the TGFβ signaling pathway and JMJD3 to co-regulate gene transcription suggests that Smad3 and JMJD3 bind a subset of common target genes. To investigate this hypothesis, we identified the genome-wide binding sites of Smad3 and JMJD3 in NSCs treated with TGFβ by sequencing DNA fragments of immunoprecipitated chromatin (ChIP-Seq) (Fig. 3A). With values normalized to the input, 98086 and 63154 peaks were detected in ChIP data for Smad3 and JMJD3, respectively. To validate the ChIP-Seq results, as well as the specificity of JMJD3 and Smad3 antibodies, we performed ChIP followed by qPCR for a representative set of Smad3 and JMJD3 target genes. Specifically, we selected: Smad3 and JMJD3 promoter targets corresponding to genes regulated at transcriptional level by Smad3 and JMJD3

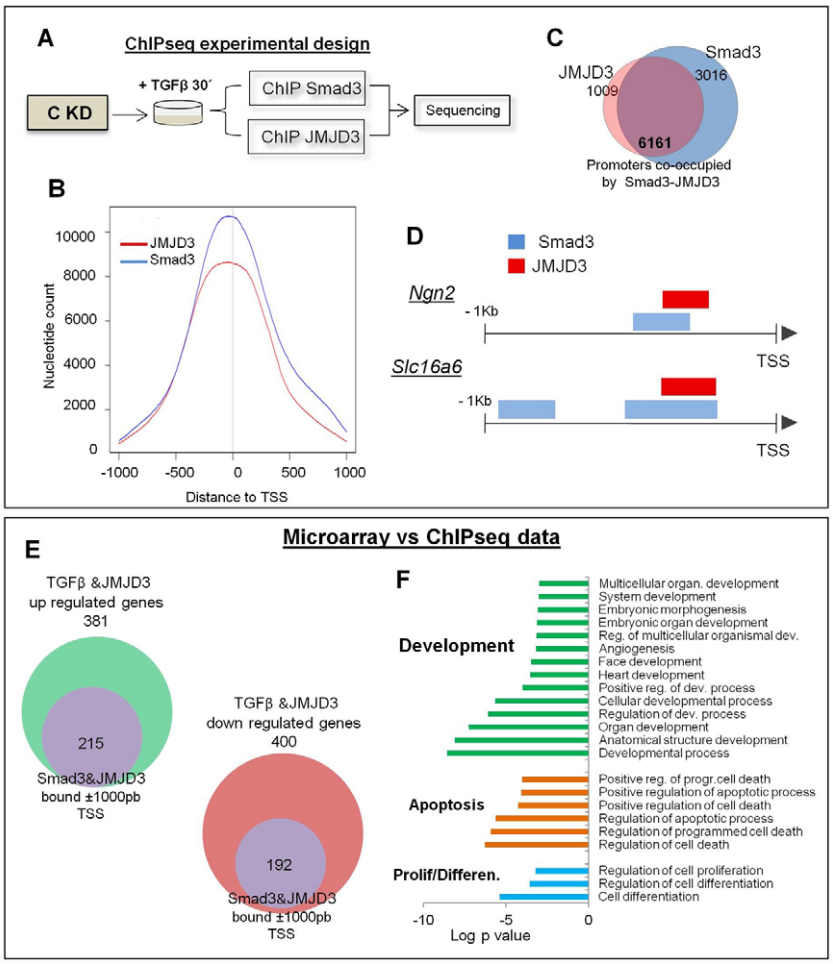

Fig. 3. Smad3 and JMJD3 colocalize on gene promoters. (**A**) ChIP-Seq experimental procedure. (**B**) Distribution of the distance of Smad3 (blue) and JMJD3 (red) peaks from the TSS. (**C**) Venn diagram showing promoters (–1000 to TSS) co-bound by Smad3 and JMJD3. (**D**) Representation based on BED files obtained for Smad3- and JMJD3-binding sites on *Ngn2* and *Slc16a6* promoters. (**E**) Venn diagrams showing genes co-bound by Smad3 and JMJD3 (±1000 bp from TSS) that are transcriptionally upregulated (on the left) or downregulated by TGFβ and JMJD3 (on the right). (**F**) GO analysis of genes co-bound by Smad3 and JMJD3 that are transcriptionally regulated by TGFβ and JMJD3 (407 targets; 215 upregulated plus 192 downregulated).

(seven upregulated and seven downregulated; supplementary material Fig. S4A,B), and four promoters of genes not regulated in the microarray experiment (supplementary material Fig. S4A,B). Finally, to test the specificity of the antibodies we chose three areas corresponding to intergenic regions occupied only by Smad3 (named IGR1, IGR2 and IGR3) and three occupied only by JMJD3 (named IGR4, IGR5 and IGR6) (supplementary material Fig. S4A,B). Then, we examined the genomic distribution of the Smad3 and JMJD3 peaks. Our results showed that both Smad3 and JMJD3 peaks are distributed across various genomic regions (supplementary material Fig. S4C), consistent with what has been found in other cell contexts (De Santa et al., 2009; Kim et al., 2011). Importantly, the overlapping regions between Smad3 and JMJD3 are mainly located around the transcription start site (TSS) (supplementary material, Fig. S4D,E), containing a common peak maximum around –100 bp from the TSS (Fig. 3B,D). As shown in Fig. 3C, 6158 promoters (–1000 to 0 bp from the TSS) were found to be targeted by both Smad3 and JMJD3.

Interestingly, of the 381 genes that showed a JMJD3 dependency for transcriptional activation in the microarray experiment, 215 (56.4%) were bound by Smad3 and JMJD3 (Fig. 3E, left panel and supplementary material Table S1). Furthermore, 192 genes out of those 400 (48%) downregulated in the microarray experiment were also direct targets of Smad3 and JMJD3 (Fig. 3E, right panel) suggesting a potential role for JMJD3 in transcriptional repression. Enrichment analysis of GO terms over these 407 (215 upregulated plus 192 downregulated) Smad3 and JMJD3 co-regulated direct targets showed that the most enriched GO terms are again associated with several different aspects of development (Fig. 3F).

Taken together, these results indicate that JMJD3 cooperates with Smad3 regulating the expression of genes involved in development.

JMJD3 permanency at promoters is independent of Smad3

To further analyze the mechanism by which TGFβ and JMJD3 cooperate to activate transcription, we studied several genes involved in development and neural function (*Slc16a6*, *Eomes*, *Ngn2*, *Ctgf* and *Stx3)* from those listed in supplementary material Table S1. First, we performed a time-course experiment of Smad3 and JMJD3 recruitment at the promoters under study. Results illustrated in Fig. 4A,B show that soon after activation (30 minutes), Smad3 and JMJD3 were recruited to the TGFβ-responsive promoters but not to the control gene *Hbb*. Three hours later, Smad3 had been displaced, but JMJD3 remained at most promoters (*Slc16a6*, *Eomes*, *Ngn2 and Ctgf*), correlating with mRNA accumulation (Fig. 4A,B,D). Given the known HDM activity of JMJD3, we wondered whether its recruitment resulted in H3K27me3 removal. It was observed that H3K27me3 levels decreased from 3 hours after TGFβ treatment in the four methylated promoters (Fig. 4C). This change was probably due to JMJD3 because no changes were detected in H3K27me3 levels in JMJD3 KD cells (supplementary material Fig. S5). However, this

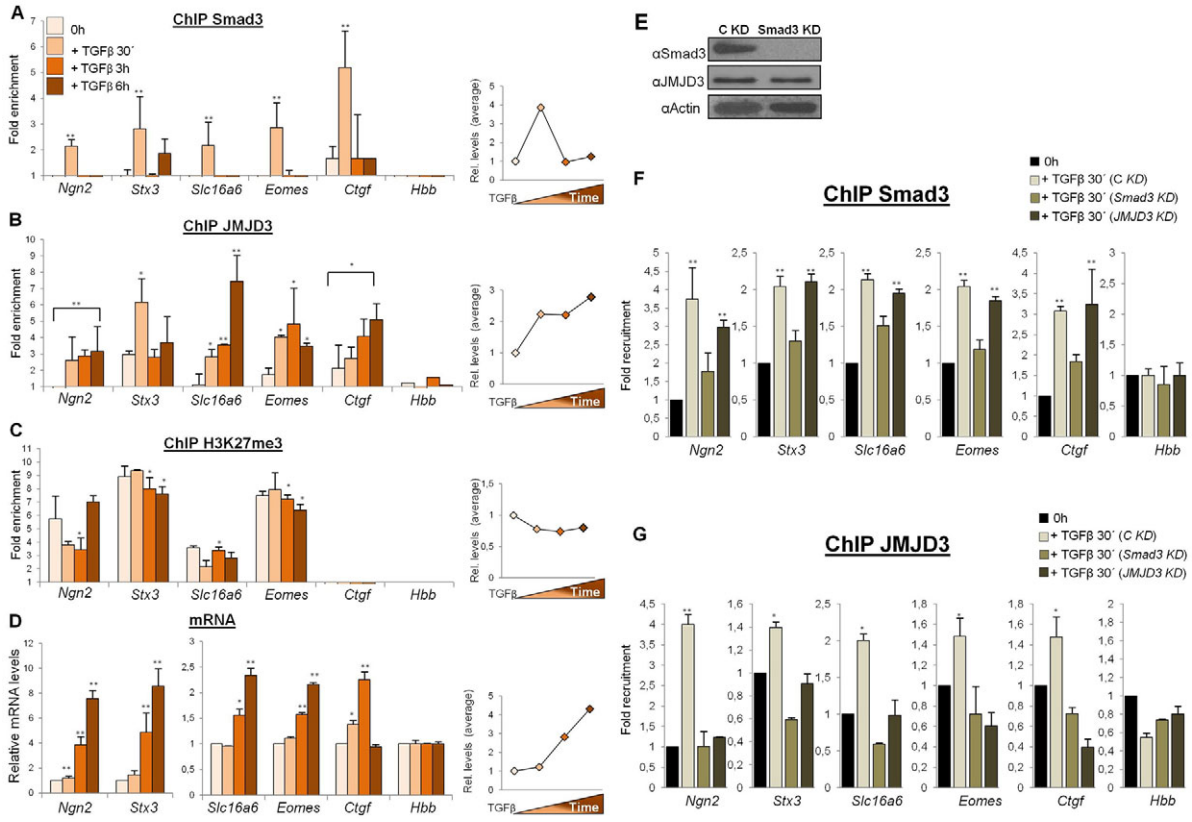

Fig. 4. Smad3 recruits JMJD3 to promoters in response to TGFβ. (**A-D**) ChIPs [of Smad3 (A), JMJD3 (B) and H3K27me3 (C)] and mRNA levels (D) analyzed by qPCR were performed in NSCs left untreated (0 hours) or treated with TGFβ (30 minutes, 3 hours or 6 hours). Graphs on the right represent the mean levels at the analyzed promoters. (**E**) Immunoblot from C KD and Smad3 KD cell extracts using the indicated antibodies. (**F**,**G**) ChIPs of Smad3 (F) and JMJD3 (G) analyzed by qPCR at the indicated promoters were performed prior to and after TGFβ treatment (30 minutes) in C KD, JMJD3 KD and Smad3 KD NSC lines (see key). ChIP results are presented as fold enrichment over a region negative for Smad3 and JMJD binding (G6pd2 gene, see supplementary material Table S2). Hbb is an additional negative control represented in the graph. Three biological replicates were used in each ChIP experiment. Data are mean±s.e.m. **P*<0.05, ***P*<0.01.

decrease was slight and not always correlated with mRNA accumulation (Fig. 4D). These data suggest that, in addition to H3K27me3 activity, other JMJD3-dependent functions might be involved in TGFβ-responsive promoter activation.

The simultaneous binding of Smad3 and JMJD3 to common targets 30 minutes after TGFβ treatment led us to investigate whether Smad3 reduction affects JMJD3 recruitment to promoters. To address this issue, we first established a Smad3-depleted NSC line (Smad3 KD), which express low levels of Smad3 protein without affecting JMJD3 expression (Fig. 4E; supplementary material Fig. S2C). Then, we analyzed the binding of Smad3 and JMJD3 in each of the three cell lines (Fig. 4F,G). We observed that Smad3 binding to the promoters increases upon TGFβ treatment in both the C KD and JMJD3 KD cell lines, whereas, as expected, the binding was severely reduced in the Smad3 KD cell line (Fig. 4F). However, JMJD3 recruitment to promoters upon TGFβ treatment was detected only in the C KD cell line (Fig. 4G).

Taken together, these findings indicate that the TGFβ pathway activates the expression of some target genes through a rapid recruitment of JMJD3 by Smad3 to the corresponding promoters. JMJD3 targeting triggers H3K27 demethylation and subsequent transcriptional initiation, whereas Smad3 is displaced and no longer required for stable JMJD3 binding. Moreover, the active recruitment of JMJD3 to the non-H3K27-methylated *Ctgf* promoter and the low decrease of H3K27me3 at methylated promoters suggests that JMJD3 may have an additional role in transcriptional activation, beyond its HDM activity on H3K27me3.

TGFβ-induced neurogenesis in the spinal cord requires JMJD3

The findings described above support the idea that Smad3, together with JMJD3, regulates genes important for neural development (Fig. 2C, Fig. 3F). Hence, we tested whether JMJD3 cooperates with the TGFβ pathway in an in vivo model of neural development, the chick embryo neural tube. Structurally, three zones can be distinguished in a transversal section of neural tube: the ventricular zone (VZ), where proliferating progenitors reside; the transition zone (TZ), where neuroblasts exit the cell cycle to initiate differentiation; and the mantle zone (MZ), where the final differentiated neurons reside (Fig. 5B). We first examined the expression domains of Smad3 and JMJD3 in developing spinal cord. In situ hybridization (ISH) of transverse sections of Hamburger and Hamilton (HH) stage 24-26 embryos showed that both mRNA were expressed in similar domains: in the dorsal part of the VZ and in the TZ (Fig. 5A,B). In addition, Smad3 immunostaining experiments show a similar distribution of active (nuclear) Smad3 (supplementary material Fig. S6). The extended colocalization of Smad3 and

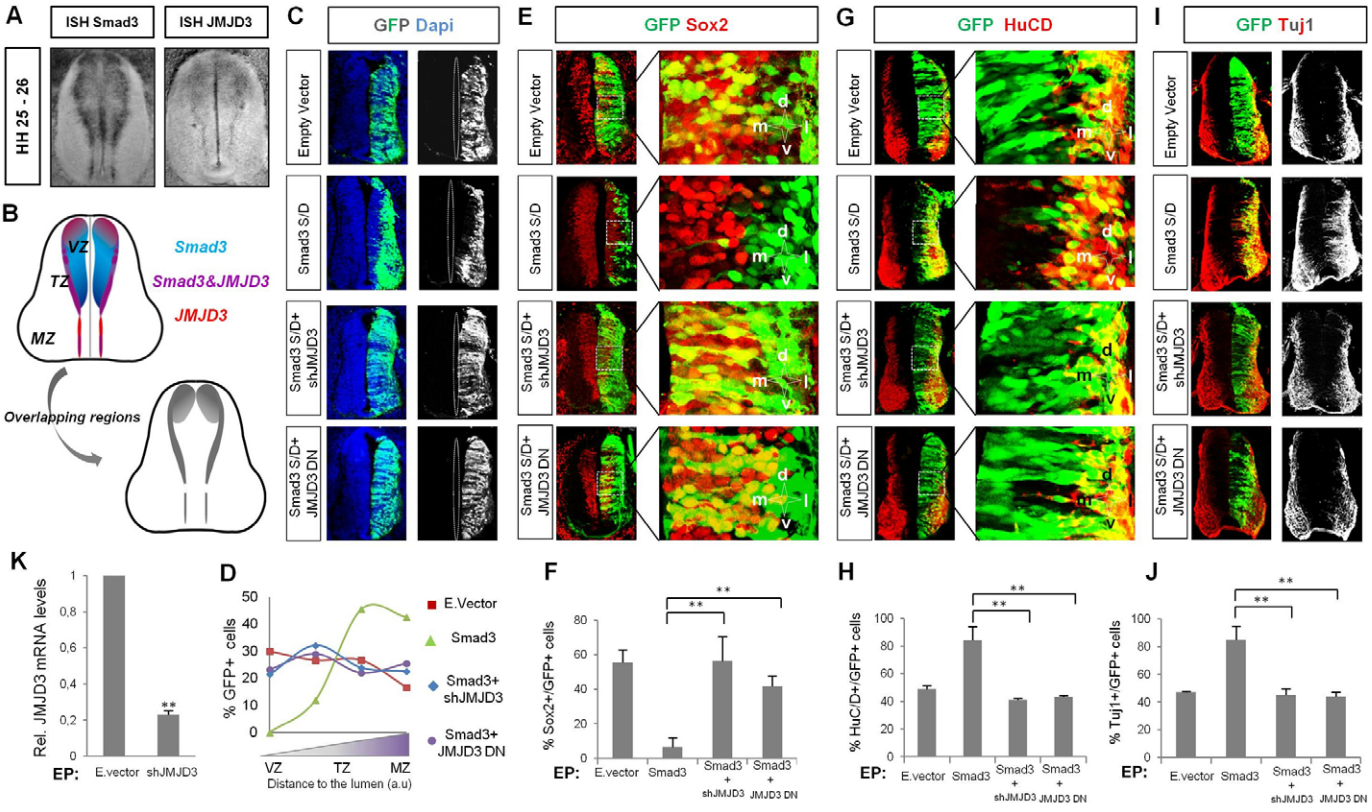

Fig. 5. Smad3 and JMJD3 cooperate to induce neuronal differentiation in chick spinal cord. (**A**) Smad3 and JMJD3 mRNA in situ hybridization in HH25-26 embryo spinal cord. (**B**) Schematic representation of Smad3 and JMJD3 expression domains shown in A. (**C**,**E**,**G**,**I**) HH12 embryos were electroporated in ovo with the DNAs (cloned into a bicistronic vector containing GFP) indicated in the vertical boxes and processed (48 hours PE) for the immunostaining indicated. The right side corresponds to the electroporated side (GFP positive). (**D**) Quantification of the lateral distribution of GFP$^+$ cells from the lumen to the mantle zone of the neural tube. (**F**,**H**,**J**) Graphs showing the percentage of electroporated cells (GFP$^+$) positive for Sox2, HuCD and Tuj1, respectively. Data are the mean of *n*=30 sections (from 4-6 embryos). (**K**) JMJD3 mRNA levels were determined by qPCR from sorted EP neural tube cells (GFP$^+$) with the empty vector (E. vector) or shRNA of JMJD3-containing vector (shJMJD3) for 48 hours. Data are mean±s.e.m. $^{**}P<0.01$.

JMJD3 along the dorsoventral axis of the TZ in the neural tube (Fig. 5A,B) and the previously reported function of Smad3 in inducing neuronal differentiation in this model (Garcia-Campmany and Marti, 2007) suggest that Smad3 and JMJD3 could functionally cooperate in developing spinal cord.

To analyze the function of the proteins of interest, we electroporated the recombinant DNAs cloned in a bicistronic vector containing GFP sequence in the neural tube; thus, the EP cells were GFP positive (GFP$^+$). It has been previously shown that overexpression of the pseudo-phosphorylated Smad3 (Smad3S/D) in the chick neural tube promotes neuronal differentiation (Garcia-Campmany and Marti, 2007) (Fig. 5C-J). The neuronal differentiation phenotype can be monitored in three ways: (1) lateral distribution of GFP-positive cells; (2) analysis of progenitor markers; and (3) neuronal differentiation marker expression. Fig. 5C,D shows that Smad3S/D in ovo EP cells differentiate earlier and, as a consequence, are mainly in the MZ of the neural tube where fully differentiated neurons are found, in contrast to the even distribution observed for the empty vector EP cells (Fig. 5C,D). In line with this, Smad3S/D EP cells are excluded from the progenitor zone stained with Sox2 marker (Fig. 5E,F), and, furthermore, express high levels of the neuronal differentiation markers HuC/D and Tuj1 (Fig. 5G-J). We then tested whether Smad3-mediated phenotype was related to JMJD3 overexpression by checking JMJD3 mRNA levels upon Smad3 electroporation, but we did not observe any increase in the transcript of the demethylase (supplementary material Fig. S7).

Next, we sought to assess the role of endogenous JMJD3 on Smad3-induced neuronal differentiation. To achieve this, we first cloned an shRNA for chick JMJD3 in a bicistronic vector containing GFP sequence, which efficiently reduces JMJD3 levels (Fig. 5K). Then, we electroporated in ovo Smad3S/D together with shJMJD3 and analyzed the previously described markers. First, we investigated the distribution of GFP$^+$ cells. In this case, co-EP GFP$^+$ cells failed to migrate to the MZ, in contrast to EP Smad3S/D cells, indicating that the lack of JMJD3 counteracts Smad3 neurogenic induction (Fig. 5C,D). Moreover, Smad3S/D and shJMJD3 co-EP cells expressed higher levels of Sox2 proliferation marker than did Smad3S/D EP cells (percentage of Sox2$^+$/GFP$^+$ cells: empty vector 55.43%, Smad3S/D 6.54%, Smad3S/D together with shRNA-JMJD3 56.26%) (Fig. 5E,F). In addition, the total number of Sox2$^+$ cells in the EP side was recovered, counteracting the global progenitors reduction promoted by Smad3 (supplementary material Fig. S8A). Furthermore, Smad3-shJMJD3 co-EP cells express fewer HuC/D and Tuj1 differentiation markers than do Smad3S/D EP cells (percentage of HuCD$^+$/GFP$^+$ cells: empty vector 48.96%, Smad3S/D 84.22%, Smad3S/D together with shRNA-JMJD3 41.24%; percentage of Tuj1+/GFP+ cells: empty vector 47.74%, Smad3S/D

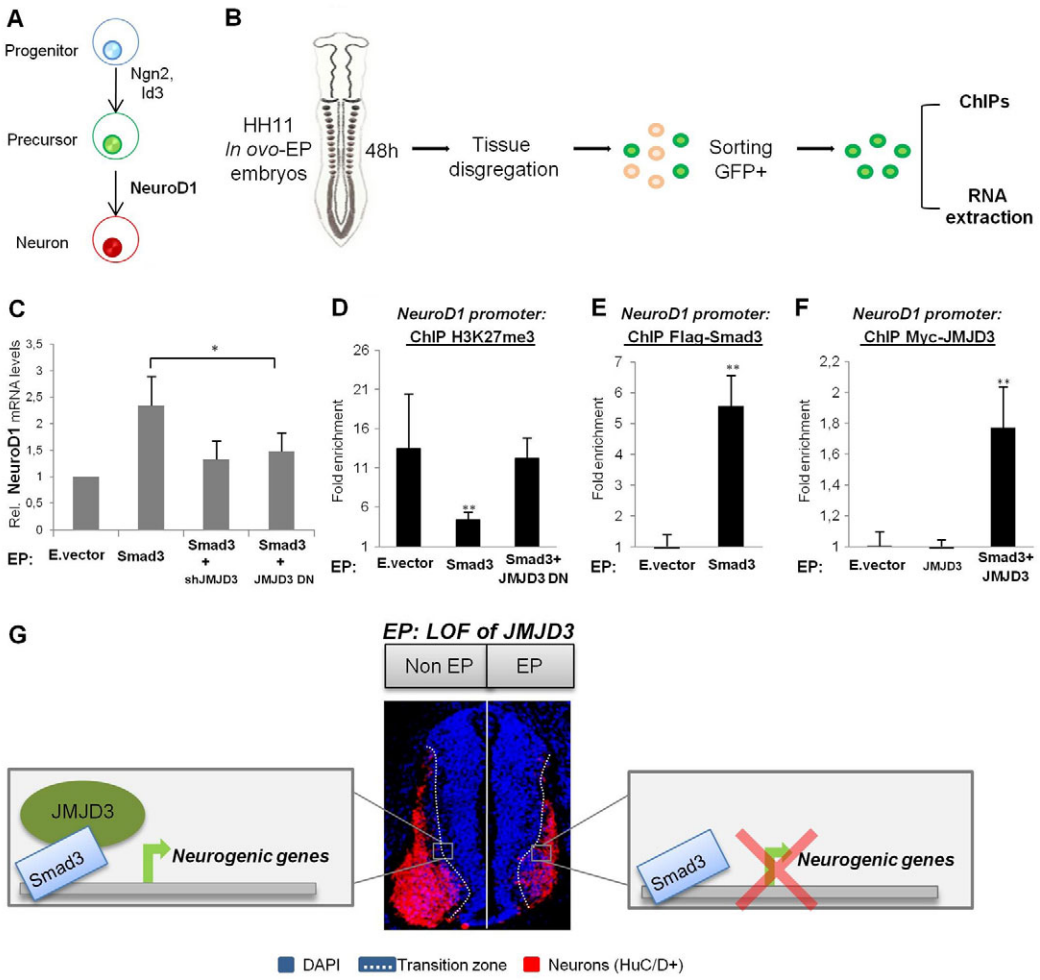

Fig. 6. *NeuroD1* is a target of Smad3 and JMJD3 in the neural tube. (**A**) Schematic representation of bHLH gene expression during neurogenesis. (**B**) Schematic representation of chick embryo RNA extraction and ChIP procedures. (**C**) *NeuroD1* mRNA levels from EP neural tube cells (GFP$^+$) with the indicated DNAs were determined by qPCR. (**D-F**) ChIPs analyzed by qPCR from EP neural tube cells (GFP+) with DNAs indicated on the *x*-axis of the graphs using H3K27me3 (C), Flag (D) and Myc (E) antibodies at the *NeuroD1* promoter. Results are represented as fold enrichment over negative binding regions for Smad3 and JMJD3 (±s.e.m.). *Tll* promoter was used as negative control for Smad3 and JMJD3 binding, and *Hes5* promoter as negative control for H3K27me3. Three biological replicates were used in each experiment. **P*<0.05, ***P*<0.01. (**G**) Schematic diagram summarizing our results. In the non-EP side of the neural tube, Smad3 drives neuronal differentiation activating the expression of neuronal genes in the TZ (such as *NeuroD1*) together with JMJD3. In the side EP with loss of function (LOF) of JMJD3, Smad3 is not able to efficiently activate proneural genes, leading a reduction in the number of differentiated neurons (see HuC/D marker in red).

85.23%, Smad3S/D together with shRNA-JMJD3 45.33%) (Fig. 5G-J; supplementary material Fig. S8C). According to the global changes observed in the progenitors population, the increase of differentiated cells (HuCD$^+$ or Tuj1$^+$) promoted by EP of Smad3S/D was impaired in Smad3-shJMJD3 co-EP neural tubes (supplementary material Fig. S8B). To further confirm the cooperation of JMJD3 with active Smad3 to induce neuronal differentiation, we performed JMJD3 gain-of-function experiments. Results in supplementary material Fig. S9 strongly support our previous results by showing that co-EP of Smad3S/P and JMJD3 wild type leads to premature and ectopic neuronal differentiation induction.

As the endogenous chick Smad3 is active (supplementary material Fig. S6) we tested the effect of loss of function of JMJD3 on endogenous neuronal differentiation. Electroporation of shJMJD3 alone had a blocking effect on endogenous neuronal differentiation (supplementary material Fig. S10A-D), that equally affects dorsal and ventral terminally differentiated neurons (supplementary material Fig. S10E-G). These results strongly indicate that JMJD3 is required for Smad3 to induce neuron generation in chick embryo spinal cord.

Next, we wondered about the correlation between the observed phenotypes and the H3K27me3 status of the EP cells. To achieve this, we checked the H3K27me3 levels of shJMJD3 and JMJD3 wild-type EP cells. Results in supplementary material Fig S11 indicate that, even though we could not detect a global increase in the H3K27me3 levels in JMJD3 depleted cells (probably owing to technical limitations), we observed a decrease in H3K27me3 signal upon EP of JMJD3 wild type. Moreover, this global demethylation promoted by JMJD3 wild type electroporation correlates with the dramatic neuronal differentiation observed when Smad3 is co-electroporated with JMJD3 wild type (supplementary material Fig. S9). Overall, these results point to an important function of JMJD3 regulating H3K27me3 levels in the neural tube.

Smad3-JMJD3 cooperation requires JMJD3 HDM activity

Based on our previous data, we assessed whether the requirement of JMJD3 for TGFβ-induced neurogenesis in developing spinal cord depends on the HDM activity mediated by the Jumonji C domain of JMJD3. To achieve this, we used a JMJD3 mutant lacking HDM activity that acts as a dominant-negative form of JMJD3 (JMJD3 DN) (Akizu et al., 2010) (supplementary material Fig. S11). Fig. 5C-J shows that co-electroporation of JMJD3 DN together with Smad3S/D, counteracts Smad3-induced neuronal differentiation, similar to the effect observed upon EP of Smad3S/D and shJMJD3. Again, electroporation of JMJD3 DN alone blocks endogenous neuronal differentiation (supplementary material Fig. S10A-G). These findings demonstrate that the demethylase activity of JMJD3 is essential for Smad3-induced neurogenesis.

NeuroD1 is regulated by Smad3 and JMJD3 HDM activity

Our data using NSCs indicates that Smad3 and JMJD3 cooperate to co-regulate genes important for neural development, among them class II bHLH genes essential for proper neurogenesis (*Ngn2* and *Id3*). bHLH activators show temporal expression sequence during central nervous system development on the basis that they can be further divided into: neural determination factors, such as the proneural genes *Mash1*, *Ngn1* and *Ngn2*, which are expressed in proliferating neural progenitors at the initiation of neuronal differentiation; and neural differentiation factors, such as *NeuroD1*, which is mainly expressed in young postmitotic neurons undergoing neuronal differentiation (Fig. 6A; supplementary material Fig. S12A). In order to investigate the implication of JMJD3 regulating the expression of late bHLH genes, we use the developing chicken neural tube where TGFβ signaling induces terminal neural differentiation and patterning specification (Garcia-Campmany and Marti, 2007). We first confirmed that the proneural gene *Ngn2* is also a TGFβ target that requires JMJD3 activity for full induction in chick neural tube. To do this, Smad3S/D, together with shJMJD3 or JMJD3 DN vector, were in ovo electroporated, the neural tubes were dissected out 24 hours later and GFP^+ cells sorted by FACS were processed for RNA extraction and analyzed by qPCR (Fig. 6B). Results in supplementary material Fig. S12B shows that, in chicken neural tube, TGFβ also induces *Ngn2* gene expression; moreover, this induction was partially blocked by overexpression of JMJD3 DN or shJMJD3, together with the TGFβ effector. Once confirmed that the proneural gene *Ngn2* is also a TGFβ and JMJD3 target in chicken neural tube, we tested whether Smad3 and JMJD3 promoted neurogenesis by co-regulating late bHLH genes, such as *NeuroD1*. To achieve this, 48 hour EP GFP^+ cells were sorted for RNA extraction or ChIP assays (Fig. 6B). Fig. 6C shows that Smad3S/D electroporation induces *NeuroD1* expression. This induction was severely counteracted by overexpression of JMJD3 DN or shJMJD3, together with the TGFβ effector (Fig. 6C). In accordance with *NeuroD1* mRNA expression levels, co-EP of JMJD3 DN blocked Smad3-induced H3K27 demethylation of the *NeuroD1* promoter (Fig. 6D). To check whether this regulation occurs through a direct binding of Smad3 and JMJD3 to *NeuroD1* promoter, we electroporated Flag-Smad3 or Myc-JMJD3 and performed ChIP assays in EP cells using Flag or Myc antibodies. Results in Fig. 6E,F show that Flag-Smad3 binds *NeuroD1* promoter, but this is not the case for Myc-JMJD3. As our previous results in NSCs indicated that JMJD3 requires Smad3 to target promoters (Fig. 4G), we electroporated Flag-Smad3 together with Myc-JMJD3 and performed a new Myc-JMJD3 ChIP assay. Results in Fig. 6F show that Myc-JMJD3 is recruited to *NeuroD1* promoter in cells co-EP with the TGFβ effector, confirming our previous results that JMJD3 targeting requires Smad3 (Fig. 4G).

Overall, our findings highlight an essential role for JMJD3 activity in Smad3-dependent neural vertebrate development through co-regulation of early (*Ngn2*) and late (*NeuroD1*) master genes for neuronal differentiation.

DISCUSSION

Our results demonstrate by genome-wide analysis and experiments in vertebrate embryos that TGFβ response is largely dependent on the Smad3 co-regulator JMJD3.

Although a large number of Smad co-factors have been previously described, how they provide specificity and plasticity to TGFβ response is still unknown. Recent studies have shown that master transcription factors, such as Oct4 in ESCs, Myod1 in myotubes and PU.1 in pro-B cells select cell-type-specific responses to TGFβ signaling (Mullen et al., 2011). Our studies expand this knowledge showing that an epigenetic regulator, not a transcription factor, determines the TGFβ outcome during development. Our results demonstrate that JMJD3 recruitment to Smad3-targeted promoters is essential for triggering the transcriptional activation of TGFβ-responsive genes that are key for development. As we have shown, JMJD3 depletion compromises the transcriptional regulation of developmental genes. Moreover, in the chick neural tube, JMJD3 is essential for Smad3-induced neuronal differentiation.

By establishing a molecular link between JMJD3 and TGFβ signaling, our study provides new insight into how a developmental signal is integrated into chromatin to provide the transcriptional plasticity required during development. In addition, our data propose that a dynamic H3K27me3 targets behavior, modulated by signal-dependent targeting, which recruits JMJD3 by DNA sequence-specific transcription factor Smad3 to neuronal genes. The knowledge about how histone demethylases are recruited to the promoter regions is very limited. It has been shown that T-box transcription factors recruit H3K27me3 demethylases to chromatin (Miller et al., 2008; Miller and Weinmann, 2009). Similarly, p53 by interacting with JMJD3 cooperates to control neurogenesis (Sola et al., 2011). Moreover, recent data have revealed that Smad2/3 and Smad1 (Akizu et al., 2010; Dahle et al., 2010; Kim et al., 2011), by interacting with JMJD3, recruit it to some loci. Our data extend these findings showing that (1) JMJD3 specifically interacts with Smad3 and (2) this association occurs in almost 7000 promoters in NSCs; moreover, (3) we demonstrate that JMJD3 is essential for Smad3 to activate transcription of key neural genes. Finally, our finding reveals that (4) TGFβ-dependent neuron generation in chick embryo spinal cord requires JMJD3 activity (Fig. 6G).

The contribution of H3K27me3 demethylation to JMJD3-mediated transcriptional activation is an intriguing issue. Our results indicate that H3K27me3 levels decrease 3 hours after TGFβ treatment in the methylated promoters (Fig. 4C). However, the active recruitment of JMJD3 to the non-H3K27-methylated like *Ctgf* promoter and the low decrease of H3K27me3 at methylated promoters, suggests that, in addition to H3K27me3 demethylation, other JMJD3-dependent functions might be involved in TGFβ-responsive promoter activation as it has been previously proposed (De Santa et al., 2009; Miller et al., 2010). Finally, our data with JMJD3 DN clearly demonstrate that HDM activity is required to facilitate TGFβ-induced neuronal differentiation, as well as to demethylate and activate the key *NeuroD1* promoter. These results

open the possibility that other essential factors different from histone H3 might be targeted by JMJD3 HDM activity upon TGFβ signaling activation. This hypothesis would explain the dependency of HDM activity on JMJD3 function and the lack of correlation with H3K27me3 levels at some analyzed promoters.

In addition to TGFβ pathway, other developmental signaling pathways might also use JMJD3 to increase the rate of transcription of responsive genes. In agreement with this idea, our laboratory has recently shown that JMJD3 regulates the BMP pathway by interacting with Smad1 in developing chick spinal cord (Akizu et al., 2010). These data raise the possibility that effectors from different signaling pathways could compete with one another for binding and recruitment of JMJD3 to a different set of genes in a particular spatial and temporal order. In line with this, JMJD3 function would depend on the combination of active signaling pathways at each developmental stage.

In summary, this study identifies a new TGFβ signaling-dependent JMJD3 regulatory function, demonstrating a role for this demethylase in neural vertebrate development. owing to the broad range of TGFβ functions in other processes such as cancer, it would now be interesting to investigate the role of TGFβ-dependent JMJD3 transcriptional regulation in other cellular contexts.

Acknowledgements

We thank Dr E. Martí, Dr K. Helin, Dr J. Christensen and K. Williams for reagents, technical assistance and helpful discussions. We also thank Dr X. Yang, Dr K. Ge, Dr J. Massagué, Dr J. Seoane, Dr J. C. Reyes and Dr S. Pons for reagents.

Funding

This study was supported by the Spanish Ministry of Education and Science [CSD2006-00049 and BFU2009-11527 to M.A.M.-B., and BFU2009-11527 and BIO2006-15557 to X.C.], by Fundaciò La Marató de TV3 [090210 to M.A.M.-B.] and by Consejo Superior de Investigaciones Científicas [200420E578 to X.C.]. C.E. and N.A. were recipients of FPU and I3P (I3P-BPD2005) fellowships, respectively.

Competing interests statement

The authors declare no competing financial interests.

Supplementary material

Supplementary material available online at
http://dev.biologists.org/lookup/suppl/doi:10.1242/dev.078345/-/DC1

References

Agger, K., Cloos, P. A., Christensen, J., Pasini, D., Rose, S., Rappsilber, J., Issaeva, I., Canaani, E., Salcini, A. E. and Helin, K. (2007). UTX and JMJD3 are histone H3K27 demethylases involved in HOX gene regulation and development. *Nature* **449**, 731-734.

Agger, K., Cloos, P. A., Rudkjaer, L., Williams, K., Andersen, G., Christensen, J. and Helin, K. (2009). The H3K27me3 demethylase JMJD3 contributes to the activation of the INK4A-ARF locus in response to oncogene- and stress-induced senescence. *Genes Dev.* **23**, 1171-1176.

Akizu, N., Estaras, C., Guerrero, L., Marti, E. and Martinez-Balbas, M. A. (2010). H3K27me3 regulates BMP activity in developing spinal cord. *Development* **137**, 2915-2925.

Blanco-Garcia, N., Asensio-Juan, E., de la Cruz, X. and Martinez-Balbas, M. A. (2009). Autoacetylation regulates P/CAF nuclear localization. *J. Biol. Chem.* **284**, 1343-1352.

Boyer, L. A., Plath, K., Zeitlinger, J., Brambrink, T., Medeiros, L. A., Lee, T. I., Levine, S. S., Wernig, M., Tajonar, A., Ray, M. K. et al. (2006). Polycomb complexes repress developmental regulators in murine embryonic stem cells. *Nature* **441**, 349-353.

Bracken, A. P., Dietrich, N., Pasini, D., Hansen, K. H. and Helin, K. (2006). Genome-wide mapping of Polycomb target genes unravels their roles in cell fate transitions. *Genes Dev.* **20**, 1123-1136.

Burgold, T., Spreafico, F., De Santa, F., Totaro, M. G., Prosperini, E., Natoli, G. and Testa, G. (2008). The histone H3 lysine 27-specific demethylase Jmjd3 is required for neural commitment. *PLoS ONE* **3**, e3034.

Calloni, G. W., Le Douarin, N. M. and Dupin, E. (2009). High frequency of cephalic neural crest cells shows coexistence of neurogenic, melanogenic, and osteogenic differentiation capacities. *Proc. Natl. Acad. Sci. USA* **106**, 8947-8952.

Cao, R., Wang, L., Wang, H., Xia, L., Erdjument-Bromage, H., Tempst, P., Jones, R. S. and Zhang, Y. (2002). Role of histone H3 lysine 27 methylation in Polycomb-group silencing. *Science* **298**, 1039-1043.

Czermin, B., Melfi, R., McCabe, D., Seitz, V., Imhof, A. and Pirrotta, V. (2002). Drosophila enhancer of Zeste/ESC complexes have a histone H3 methyltransferase activity that marks chromosomal Polycomb sites. *Cell* **111**, 185-196.

Dahle, O., Kumar, A. and Kuehn, M. R. (2010). Nodal signaling recruits the histone demethylase Jmjd3 to counteract polycomb-mediated repression at target genes. *Sci. Signal.* **3**, ra48.

De Santa, F., Totaro, M. G., Prosperini, E., Notarbartolo, S., Testa, G. and Natoli, G. (2007). The histone H3 lysine-27 demethylase Jmjd3 links inflammation to inhibition of polycomb-mediated gene silencing. *Cell* **130**, 1083-1094.

De Santa, F., Narang, V., Yap, Z. H., Tusi, B. K., Burgold, T., Austenaa, L., Bucci, G., Caganova, M., Notarbartolo, S., Casola, S. et al. (2009). Jmjd3 contributes to the control of gene expression in LPS-activated macrophages. *EMBO J.* **28**, 3341-3352.

Feng, X. H. and Derynck, R. (2005). Specificity and versatility in tgf-beta signaling through Smads. *Annu. Rev. Cell Dev. Biol.* **21**, 659-693.

Frank, S. R., Schroeder, M., Fernandez, P., Taubert, S. and Amati, B. (2001). Binding of c-Myc to chromatin mediates mitogen-induced acetylation of histone H4 and gene activation. *Genes Dev.* **15**, 2069-2082.

Fujita, P. A., Rhead, B., Zweig, A. S., Hinrichs, A. S., Karolchik, D., Cline, M. S., Goldman, M., Barber, G. P., Clawson, H., Coelho, A. et al. (2011). The UCSC Genome Browser database: update 2011. *Nucleic Acids Res.* **39**, D876-D882.

Garcia-Campmany, L. and Marti, E. (2007). The TGFbeta intracellular effector Smad3 regulates neuronal differentiation and cell fate specification in the developing spinal cord. *Development* **134**, 65-75.

Gentleman, R. C., Carey, V. J., Bates, D. M., Bolstad, B., Dettling, M., Dudoit, S., Ellis, B., Gautier, L., Ge, Y., Gentry, J. et al. (2004). Bioconductor: open software development for computational biology and bioinformatics. *Genome Biol.* **5**, R80.

Gordon, K. J. and Blobe, G. C. (2008). Role of transforming growth factor-beta superfamily signaling pathways in human disease. *Biochim. Biophys. Acta* **1782**, 197-228.

Gossrau, G., Thiele, J., Konang, R., Schmandt, T. and Brustle, O. (2007). Bone morphogenetic protein-mediated modulation of lineage diversification during neural differentiation of embryonic stem cells. *Stem Cells* **25**, 939-949.

Jepsen, K., Solum, D., Zhou, T., McEvilly, R. J., Kim, H. J., Glass, C. K., Hermanson, O. and Rosenfeld, M. G. (2007). SMRT-mediated repression of an H3K27 demethylase in progression from neural stem cell to neuron. *Nature* **450**, 415-419.

Kim, S. W., Yoon, S. J., Chuong, E., Oyolu, C., Wills, A. E., Gupta, R. and Baker, J. (2011). Chromatin and transcriptional signatures for Nodal signaling during endoderm formation in hESCs. *Dev. Biol.* **357**, 492-504.

Kojima, S., Vignjevic, D. and Borisy, G. G. (2004). Improved silencing vector co-expressing GFP and small hairpin RNA. *Biotechniques* **36**, 74-79.

Kouzarides, T. (2007). Chromatin modifications and their function. *Cell* **128**, 693-705.

Kuzmichev, A., Nishioka, K., Erdjument-Bromage, H., Tempst, P. and Reinberg, D. (2002). Histone methyltransferase activity associated with a human multiprotein complex containing the Enhancer of Zeste protein. *Genes Dev.* **16**, 2893-2905.

Lan, F., Bayliss, P. E., Rinn, J. L., Whetstine, J. R., Wang, J. K., Chen, S., Iwase, S., Alpatov, R., Issaeva, I., Canaani, E. et al. (2007). A histone H3 lysine 27 demethylase regulates animal posterior development. *Nature* **449**, 689-694.

Langmead, B., Trapnell, C., Pop, M. and Salzberg, S. L. (2009). Ultrafast and memory-efficient alignment of short DNA sequences to the human genome. *Genome Biol.* **10**, R25.

Lee, M. G., Wynder, C., Bochar, D. A., Hakimi, M. A., Cooch, N. and Shiekhattar, R. (2006). Functional interplay between histone demethylase and deacetylase enzymes. *Mol. Cell. Biol.* **26**, 6395-6402.

Lee, M. G., Villa, R., Trojer, P., Norman, J., Yan, K. P., Reinberg, D., Di Croce, L. and Shiekhattar, R. (2007). Demethylation of H3K27 regulates polycomb recruitment and H2A ubiquitination. *Science* **318**, 447-450.

Lois, S., Akizu, N., de Xaxars, G. M., Vazquez, I., Martinez-Balbas, M. and de la Cruz, X. (2010). Characterization of structural variability sheds light on the specificity determinants of the interaction between effector domains and histone tails. *Epigenetics* **5**, 137-148.

Margueron, R. and Reinberg, D. (2010). Chromatin structure and the inheritance of epigenetic information. *Nat. Rev. Genet.* **11**, 285-296.

Massague, J. (2000). How cells read TGF-beta signals. *Nat. Rev. Mol. Cell Biol.* **1**, 169-178.

Massague, J., Seoane, J. and Wotton, D. (2005). Smad transcription factors. *Genes Dev.* **19**, 2783-2810.

Miller, S. A. and Weinmann, A. S. (2009). An essential interaction between T-box proteins and histone-modifying enzymes. *Epigenetics* **4**, 85-88.
Miller, S. A., Huang, A. C., Miazgowicz, M. M., Brassil, M. M. and Weinmann, A. S. (2008). Coordinated but physically separable interaction with H3K27-demethylase and H3K4-methyltransferase activities are required for T-box protein-mediated activation of developmental gene expression. *Genes Dev.* **22**, 2980-2993.
Miller, S. A., Mohn, S. E. and Weinmann, A. S. (2010). Jmjd3 and UTX play a demethylase-independent role in chromatin remodeling to regulate T-box family member-dependent gene expression. *Mol. Cell* **40**, 594-605.
Morey, L. and Helin, K. (2010). Polycomb group protein-mediated repression of transcription. *Trends Biochem. Sci.* **35**, 323-332.
Morgan, M., Anders, S., Lawrence, M., Aboyoun, P., Pages, H. and Gentleman, R. (2009). ShortRead: a bioconductor package for input, quality assessment and exploration of high-throughput sequence data. *Bioinformatics* **25**, 2607-2608.
Moustakas, A. and Heldin, C. H. (2009). The regulation of TGFbeta signal transduction. *Development* **136**, 3699-3714.
Mullen, A. C., Orlando, D. A., Newman, J. J., Loven, J., Kumar, R. M., Bilodeau, S., Reddy, J., Guenther, M. G., DeKoter, R. P. and Young, R. A. (2011). Master transcription factors determine cell-type-specific responses to TGF-beta signaling. *Cell* **147**, 565-576.
Pan, G., Tian, S., Nie, J., Yang, C., Ruotti, V., Wei, H., Jonsdottir, G. A., Stewart, R. and Thomson, J. A. (2007). Whole-genome analysis of histone H3 lysine 4 and lysine 27 methylation in human embryonic stem cells. *Cell Stem Cell* **1**, 299-312.
Rubinson, D. A., Dillon, C. P., Kwiatkowski, A. V., Sievers, C., Yang, L., Kopinja, J., Rooney, D. L., Zhang, M., Ihrig, M. M., McManus, M. T. et al. (2003). A lentivirus-based system to functionally silence genes in primary mammalian cells, stem cells and transgenic mice by RNA interference. *Nat. Genet.* **33**, 401-406.
Salmon-Divon, M., Dvinge, H., Tammoja, K. and Bertone, P. (2010). PeakAnalyzer: genome-wide annotation of chromatin binding and modification loci. *BMC Bioinformatics* **11**, 415.
Sasaki, T., Ito, Y., Bringas, P., Jr, Chou, S., Urata, M. M., Slavkin, H. and Chai, Y. (2006). TGFbeta-mediated FGF signaling is crucial for regulating cranial neural crest cell proliferation during frontal bone development. *Development* **133**, 371-381.
Schaeren-Wiemers, N. and Gerfin-Moser, A. (1993). A single protocol to detect transcripts of various types and expression levels in neural tissue and cultured cells: in situ hybridization using digoxigenin-labelled cRNA probes. *Histochemistry* **100**, 431-440.
Sen, G. L., Webster, D. E., Barragan, D. I., Chang, H. Y. and Khavari, P. A. (2008). Control of differentiation in a self-renewing mammalian tissue by the histone demethylase JMJD3. *Genes Dev.* **22**, 1865-1870.
Shi, Y. and Massague, J. (2003). Mechanisms of TGF-beta signaling from cell membrane to the nucleus. *Cell* **113**, 685-700.
Sola, S., Xavier, J. M., Santos, D. M., Aranha, M. M., Morgado, A. L., Jepsen, K. and Rodrigues, C. M. (2011). p53 interaction with JMJD3 results in its nuclear distribution during mouse neural stem cell differentiation. *PLoS ONE* **6**, e18421.
Valls, E., de la Cruz, X. and Martinez-Balbas, M. A. (2003). The SV40 T antigen modulates CBP histone acetyltransferase activity. *Nucleic Acids Res.* **31**, 3114-3122.
Varga, A. C. and Wrana, J. L. (2005). The disparate role of BMP in stem cell biology. *Oncogene* **24**, 5713-5721.
Xi, Q., He, W., Zhang, X. H., Le, H. V. and Massague, J. (2008). Genome-wide impact of the BRG1 SWI/SNF chromatin remodeler on the transforming growth factor beta transcriptional program. *J. Biol. Chem.* **283**, 1146-1155.
Xu, L., Alarcon, C., Col, S. and Massague, J. (2003). Distinct domain utilization by Smad3 and Smad4 for nucleoporin interaction and nuclear import. *J. Biol. Chem.* **278**, 42569-42577.
Yang, L. and Moses, H. L. (2008). Transforming growth factor beta: tumor suppressor or promoter? Are host immune cells the answer? *Cancer Res.* **68**, 9107-9111.
Zhang, Y., Liu, T., Meyer, C. A., Eeckhoute, J., Johnson, D. S., Bernstein, B. E., Nusbaum, C., Myers, R. M., Brown, M., Li, W. et al. (2008). Model-based analysis of ChIP-Seq (MACS). *Genome Biol.* **9**, R137.